AMERICAN SOCIETY of
GENE & CELL
THERAPY

A Discovery of Clinically Approved Formula FBRP for Repositioning to Treat HCC by Inhibiting PI3K/AKT/NF-κB Activation

Yanqiong Zhang,[1] Xia Mao,[1] Wenjia Chen,[1] Xiaodong Guo,[2] Liangxiang Yu,[2] Funeng Jiang,[3] Xiaoyue Wang,[1] Weijie Li,[1] Qiuyan Guo,[1] Taixian Li,[1] and Na Lin[1]

[1]Institute of Chinese Materia Medica, China Academy of Chinese Medical Sciences, Beijing 100700, China; [2]302 Military Hospital, Beijing 100039, China; [3]The First Affiliated Hospital of Guangzhou Medical University, Guangzhou Medical University, Guangzhou 510230, China

Drug repositioning offers new clinical applications for existing drugs with shorter approval processes and lower costs and risks than *de novo* experimental drug development. The Fufang-Bie-jia-Ruangan pill (FBRP) is the first clinically approved anti-fibrosis herbal formula in China. Whether FBRP could be used to treat hepatocellular carcinoma (HCC) remains unclear. Herein, a total of 161 FBRP candidate targets against HCC were identified according to the topological importance in the "hepatic fibrosis-cirrhosis-cancer axis-related gene-FBRP putative target" network, and mostly enriched in phosphatidy-linositol 3-kinase (PI3K)/AKT/nuclear factor κB (NF-κB) signaling. Experimentally, FBRP inhibited liver fibrosis and prevented the development of neoplastic lesions at the early stages of hepatocarcinogenesis in a diethylnitrosamine-induced rat HCC model. FBRP inhibited tumor cell proliferation, induced tumor-specific cell death, and suppressed tumor progression in HCC rats while preventing the activation of PI3K, AKT and IKKB proteins, reducing the nuclear accumulation of NFKB1 protein, and decreasing the downstream expression of proteins. Consistently, FBRP suppressed HCC cell proliferation and induced cell cycle arrest *in vitro*. Co-treatment of FBRP with PI3K inhibitor exhibited an additive inhibitory effect on PI3K/AKT/NF-κB activation. Collectively, our data showed the potentials of FBRP in hepatic fibrosis microenvironment regulation and tumor prevention, suggesting that FBRP may be a promising candidate drug for reduction of fibrogenesis and prevention of HCC.

INTRODUCTION

Drug repositioning, identifying new clinical indications for approved therapeutic drugs, has become an attractive alternative to *de novo* experimental drug development with shorter approval processes and lower costs and risks because pharmacokinetic and safety data are already available.[1] There have been various methods for drug repositioning with their own advantages and disadvantages. For example, some methods explore the new drug indication by using the chemical structural information based on the idea that molecularly similar drug structures tend to share common indications and affect biological systems in similar ways.[2–4] However, growing evidence shows that drugs with

similar structures may also target proteins with different functions, implying that just using chemical structure alone may be insufficient for successful drug repositioning.[5] Alternatively, many computational approaches investigate the effects of a repositioned drug by analyzing drug phenotype-related expression signatures. The key assumption of such approaches may be that drugs that share similar expression signatures have similar therapeutic applications, but the signatures expressed in the drug-treated disease cell line or tissue cannot represent all of the molecular changes during the development and progression of complex diseases such as cancer.[6,7] To overcome the above limitations, we developed an integrated network-based computational drug repositioning approach that comprehensively incorporates disease-related genes (disease phenotype profile), drug targets (drug profile), as well as biological molecular interactions and pathways (function profile). In brief, the drug putative targets were predicted based on the chemical structures and molecular functions. Then, the "disease-related gene-drug putative target" interaction network was constructed using the links between the disease-related genes and the drug putative targets to understand the associations of the drug putative targets across disease phenotypes. After that, the functional network modules with topological importance were screened by computational approaches and subsequently identified the key drug targets against the specific disease. These efforts may lead to more efficient identification of drug targets for drug repurposing and for understanding the underlying pharmacological mechanisms of the drug.

Hepatocellular carcinoma (HCC) causes one of the highest cancer-related mortalities worldwide, accounting for approximately 90% of all hepatic malignancies in adults.[8] Although recent advances in

several therapeutic strategies, such as hepatic resection, transcatheter arterial chemoembolization (TACE), sorafenib, and transplantation, have improved the prognosis of HCC patients, about 600,000 people die yearly due to the aggressive progression of HCC.[9] The lack of efficient therapeutic options and the poor prognosis of patients have urged the development of new drugs for HCC treatment. The cause of HCC is multifactorial, and the hepatic fibrosis-cirrhosis-cancer axis is the common pathway for the vast majority of cases.[10] Therefore, the ideal treatment for HCC should be a drug that can reduce hepatic fibrosis and cirrhosis, as well as alleviate HCC.

Traditional Chinese medicine (TCM) is a comprehensive medical system that originated from ancient medical practice. TCM plays a crucial role in maintaining the health of Asian people by using herbal prescriptions, acupuncture, diet therapy, massage, and exercise to maintain the state of equilibrium of the body.[11–13] The Fufang-Biejia-Ruangan pill (FBRP) is the first clinically approved anti-fibrosis TCM prescription in China, and it has been extensively used in the treatment of hepatic fibrosis with satisfying clinical efficacy.[14] FBRP consists of 11 medicines, including *Trionycis Carapax* (BieJia [BJ]); *Paeoniae Radix Rubra* (ChiShao [CS]); *Cordyceps* (DongChongXiaCao [DCXC]); *Notoginseng Radix et Rhizoma* (SanQi [SQ]); *Hominis Placenta* (ZiHeChe [ZHC]); *Forsythiae Fructus* (LianQiao [LQ]); *Angelicae Sinensis Radix* (DangGui [DG]); *Curcumae Rhizoma* (EZhu [EZ]); *Codonopsis Radix* (DangShen [DS]); *Astragali Radix* (HuangQi [HQ]); and *Isatidis Radix* (BanLanGen [BLG]). The chemical constituents of FBRP, as well as their absorption and distribution *in vivo*, have been identified by Xiao and colleagues.[15] It has been reported to exert various pharmacological actions, such as inhibiting collagen deposition, improving liver function, and alleviating hepatic injury.[16–18] However, whether FBRP could be used for the treatment of HCC remains unclear, which restricts its clinical application and further development. Thus, in the present study, we aimed to reposition FBRP as a potential therapeutic candidate for HCC and also investigate its underlying pharmacological mechanisms using an integrated network-based computational and experimental workflow (Figure 1). At first, putative targets of candidate bioactive components containing FBRP were predicted based on their functional and structural similarities to the known US Food and Drug Administration (FDA)-approved drugs. Following the construction of the "disease gene-drug target" network using links between hepatic fibrosis-cirrhosis-cancer axis-related genes and FBRP putative targets, FBRP candidate targets against HCC were screened by analyzing network topological features and function modules. After that, the anti-HCC effect of FBRP and its regulation on the candidate target pathway were validated based on the rat hepatocarcinogenesis model induced by diethylnitrosamine (DEN), which shows severe hepatic fibrosis and generation of HCC *in vivo*, and on the HCC cell line *in vitro*.

RESULTS

Target Prediction Results Show That FBRP May Have the Potential to Treat HCC

To understand the association between FBRP and the hepatic fibrosis-cirrhosis-cancer axis at the molecular level, we first predicted the puta-tive target list of the candidate bioactive components containing FBRP (drug-likeness score of >0.49 based on the Encyclopedia of Traditional Chinese Medicine [ETCM] data;[19] http://www.nrc.ac.cn:9090/ETCM/) using a computational prediction tool, MedChem Studio. As shown in Table S1, a total of 1,348 putative targets hitting 157 candidate bioactive components of FBRP were predicted. Among the FBRP putative targets, ABCC2, CYP2B6, CYP2C19, CYP2D6, CYP3A4, CYP3A5, and CYP3A7 are the targets of sorafenib, which has received a "fast track" designation by the FDA for the treatment of advanced HCC (primary liver cancer), and has since performed well in phase III trials.[20] In addition, an orally administered inhibitor of multiple kinases, regorafenib,[21] that was approved to be expanded to treat HCC in April 2017 shares three targets (CYP2B6, CYP2C19, and CYP3A4) with FBRP.

To reveal the biological processes and pathways involving FBRP putative targets during the progression of inflammation-fibrosis-tumorigenesis transformation, we performed enrichment analysis based on Gene Ontology (GO) and the Kyoto Encyclopedia of Genes and Genomes (KEGG) pathway. The significantly enriched biological processes included metabolism-related terms, such as the oxidation-reduction process, mitochondrial electron transport, mitochondrial respiratory chain complex I assembly, regulation of the fatty acid metabolic process and lipid metabolic process, as well as inflammation and tumorigenesis-related terms, such as regulation of the inflammatory response, regulation of chemokine production, activation of mitogen-activated protein kinase (MAPK) activity, regulation of nuclear factor κB (NF-κB) transcription factor activity, regulation of NF-κB import into nucleus, regulation of the apoptotic process, and regulation of angiogenesis (all p < 0.05, Table S2). In addition, there were three significantly overrepresented pathway modules, including metabolic pathways (such as oxidative phosphorylation, glycolysis/gluconeogenesis, the citrate cycle, fatty acid degradation, and the cyclic AMP [cAMP] signaling pathway), immune system pathways (FcεRI signaling pathway, T/B cell receptor signaling pathway, Toll-like receptor signaling pathway), and cancer-related pathways (such as chemical carcinogenesis, HIF-1 signaling pathway, vascular endothelial growth factor [VEGF] signaling pathway, mammalian target of rapamycin [mTOR] signaling pathway, MAPK signaling pathway, pathways in cancer, and NF-κB signaling pathway) (all p < 0.05, Table S3). These significant data of GO and KEGG enrichment analyses indicate that the FBRP putative targets may characterize the underlying molecular basis of inflammation-fibrosis-tumorigenesis transformation.

Network-Based Drug Repositioning Results Show that FBRP May Regulate Several Key Pathways Involved in the Hepatic Fibrosis-Cirrhosis-Cancer Axis

Network-based drug repositioning analysis can contribute to identifying the relationship of drug targets with disease genes and pathways and to systematically prioritize candidate drug targets for specific diseases, therefore boosting the discovery of new drug candidates. In the current study, the disease gene-drug target network using links between hepatic fibrosis-cirrhosis-cancer axis-related genes and FBRP putative targets was constructed, and the topological importance of each node in
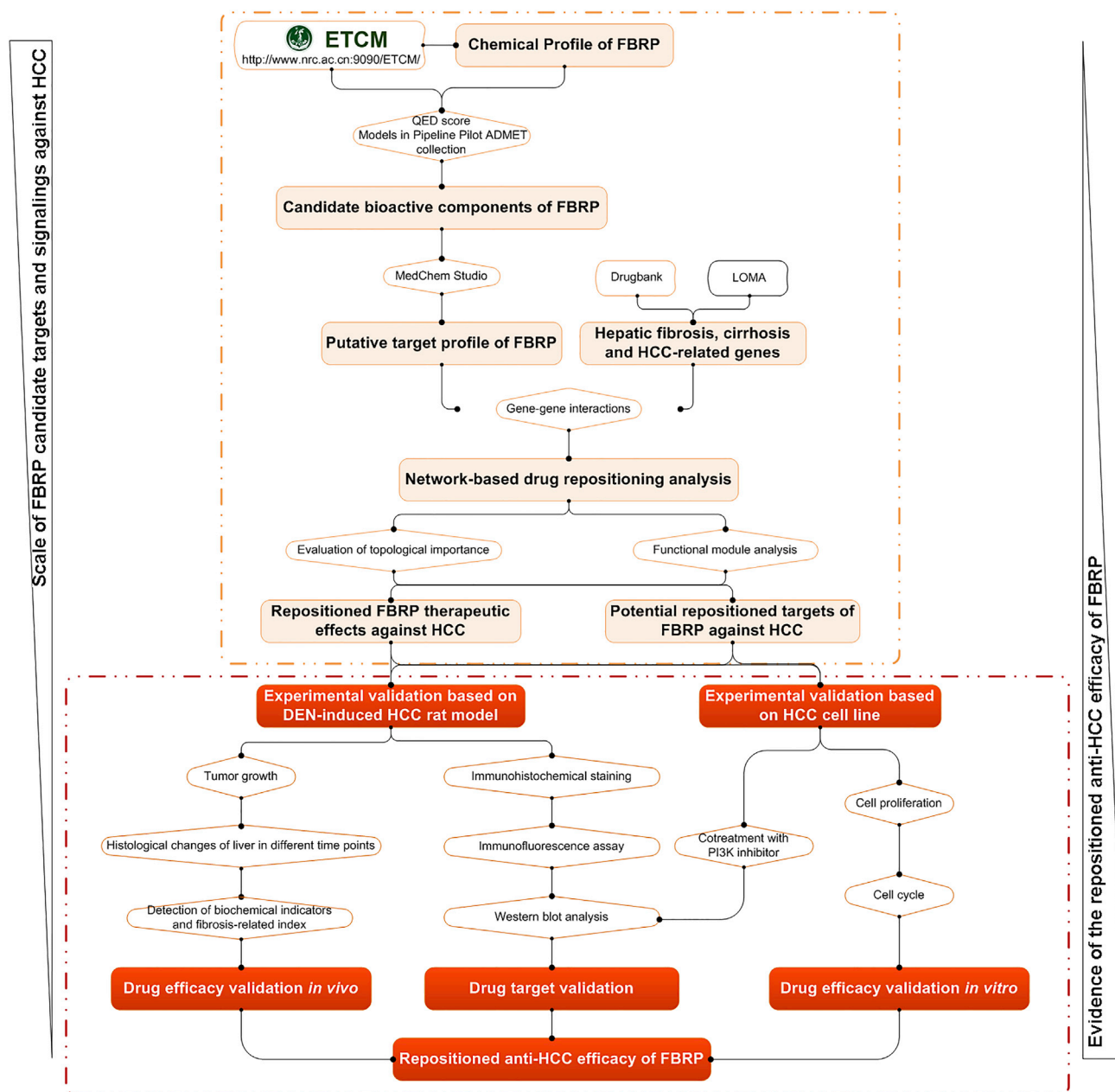
Figure 1. Schematic Diagram of Our Systematic Strategies for Drug Reposition of FBRP

the network was evaluated by calculating its degree, betweenness, and closeness. As a result, there were 411 key network targets with the high topological importance (the values of the node degree, betweenness, closeness, and k-coreness are all higher than the corresponding median). Among them, 161 were FBRP putative targets, which were indicated as FBRP candidate targets against HCC. The topological features of the key network targets are provided in Table S4.

To further identify drug target genes responsible to reverse the hepatic fibrosis-cirrhosis-cancer transformation, we divided 161 FBRP candi-

date targets against HCC into three functional modules, which were respectively associated with carcinogenesis, immune regulation and inflammation, and metabolism, according to their interconnectivity within the network using the Markov clustering algorithm (Figure 2). Among them, the carcinogenesis-related module was the top one in which FBRP candidate targets were the most involved, implying the anti-cancer potentials of FBRP. Moreover, most of the FBRP candidate targets against HCC were significantly enriched into the phosphatidylinositol 3-kinase (PI3K)-Akt signaling pathway and cell cycle, both of which play crucial roles in the regulation of tumor cell growth,
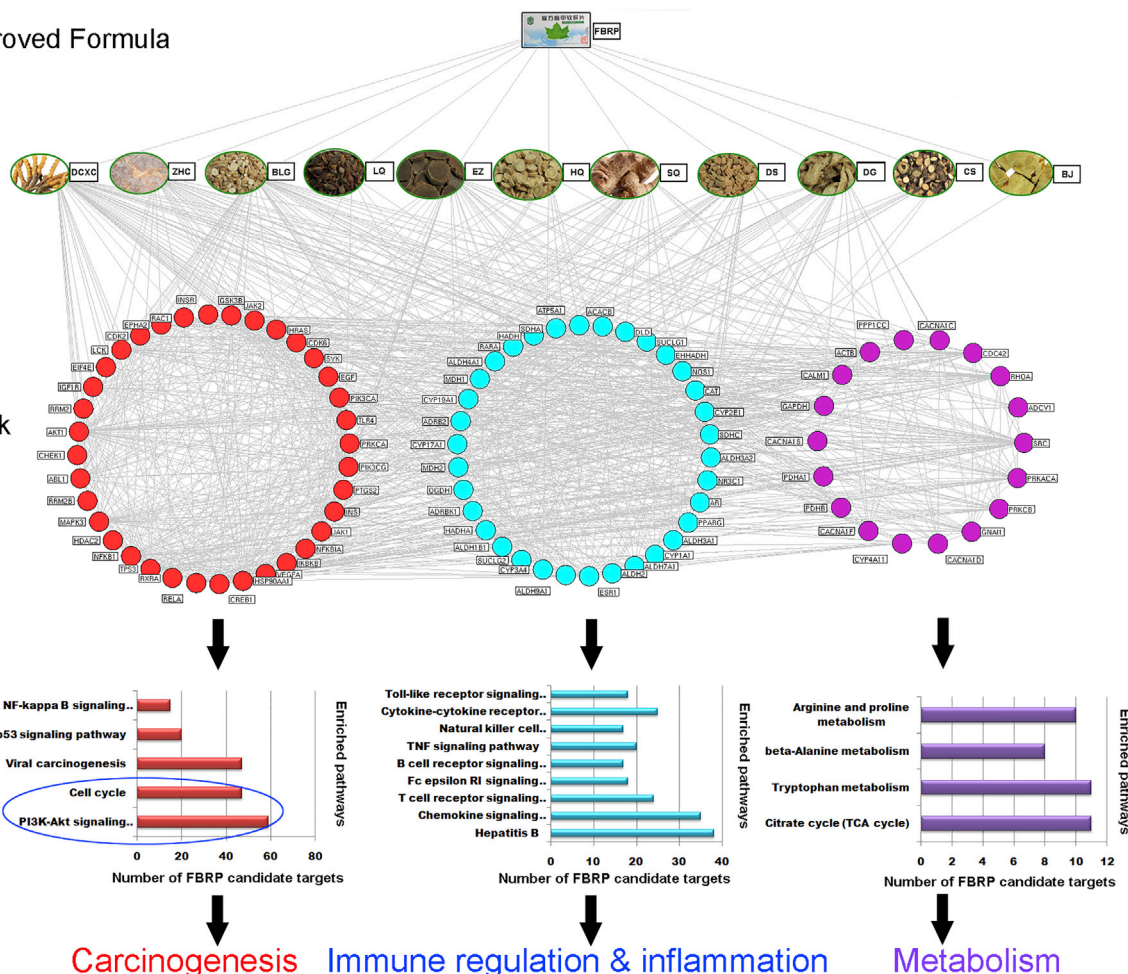
Figure 2. Network Illustration of the Associations among FBRP, Herbs, FBRP Candidate Targets against HCC, and Their Significantly Enriched Functional Modules, which Were Respectively Associated with Carcinogenesis, Immune Regulation, and Inflammation, as well as Tumor Metabolism

proliferation, apoptosis, survival, metastasis, and invasion and have been already proven to be dysregulated in HCC.[22,23] As shown in Figure 3, which illustrates the signaling transduction among FBRP candidate targets involved in the PI3K-Akt signaling pathway, the activation of PI3K and AKT may contribute to the activation of NF-κB, which functions as a common dimeric transcription factor by regulating the expression of a variety of critical genes involved in cell proliferation, apoptosis, survival, and immune responses,[24,25] and the crosstalk between them may be mediated via the signaling transducer IκB kinases (IKKs). Several cell proliferation and cell cycle-associated genes and regulatory proteins, such as cyclin D1 (CCND1), cyclin E1 (CCNE1), cyclin-dependent kinase 2 (CDK2), and cyclin-dependent kinase 4 (CDK4), may be the downstream molecules activated or regulated by NF-κB in tumor cells. The above computational investigation findings prompt us to experimentally validate the reverse effects of FBRP in the hepatic fibrosis-cirrhosis-cancer transformation as well as its regulatory effects in PI3K/AKT/NF-κB signaling, which are discussed in the following sections.

FBRP Inhibits Generation of Neoplastic Lesions, Improves Associated Fibrosis, and Prolongs Survival of DEN-Induced HCC Rats

To verify the hypothesis that FBRP could improve fibrosis progression and prevent the generation of HCC, we evaluated the therapeutic effects of FBRP based on a stable rat model with the progression of hepatic fibrosis-cirrhosis-cancer induced by DEN. During the administration of DEN, five rats from the model group died of liver function failure, while no rats died with the administration of FBRP. As shown in Figure 4A, DEN injury in rats caused progressive liver fibrosis and cirrhosis followed by HCC. In detail, repeated administration of DEN for 8 weeks caused fibrosis, and the advanced fibrosis and cirrhosis occurred after 12 weeks. By 18 weeks of DEN injury, all rats had marked neoplastic lesions. There were multiple white nodules on the surface of the livers treated with DEN, which were also demonstrated to be HCC in the following histological analyses. Notably, the administration of FBRP exhibited significant inhibition of fibrosis progression and liver neoplastic generation in DEN injury rats.
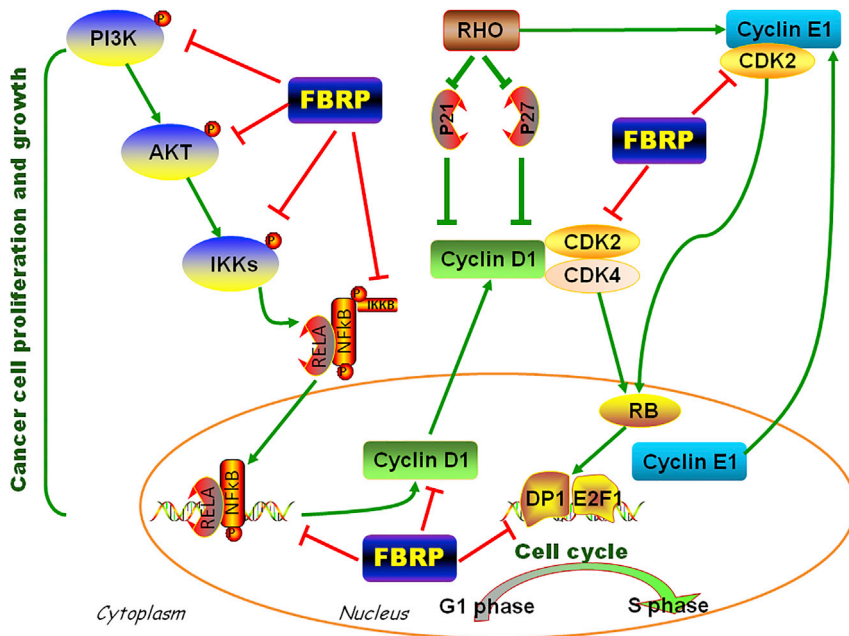
decreased level of inflammation and malignant changes at the different time points (Figure 5A).

FBRP Inhibits Liver Function-Related Serum Parameters, as well as Fibrosis and Tumor-Related Serum Markers of DEN-Induced HCC Rats

Serum levels of transaminase alanine aminotransferase (ALT), aspartate transaminase (AST), and alkaline phosphatase (ALP) in the DEN model group were significantly higher than those in the normal control and normal-FBRP groups (all $p < 0.05$, Figures 5B–5D), and they maintained a high level until 18 weeks, suggesting the liver injury induced by DEN. Compared to the normal control and normal-FBRP groups, the DEN model rats had an increased serum total protein (TP) level from week 15 to week 18 (all $p < 0.01$, Figure 5E). After beginning administration of DEN, serum fibrosis marker hyaluronic acid (HA) was high and statistically significant from week 4 to week 18 (all $p < 0.05$, Figure 5G). A gradual increase of the tumor-related serum marker alpha fetoprotein (AFP) was observed from week 12, and its serum levels were significantly higher than the normal control and normal-FBRP groups (all $p < 0.001$, Figure 5H). Importantly, the treatment of FBRP effectively reduced the increasing serum levels of ALT, AST, ALP, TP, HA, and AFP that were induced by DEN administration (all $p < 0.05$, $p < 0.01$, $p < 0.001$, Figures 5B–5H). However, no obvious alterations were observed between different groups in terms of albumin (ALB) (all $p > 0.05$, Figure 5F).

Body weight values of rats in the DEN injury model and DEN-FBRP treatment groups were markedly reduced when compared with the normal control group and the normal-FBRP group at various time points (all $p < 0.05$, Figure 4B). There were no significant differences in body weight and the liver index between normal and normal-FBRP groups, as well as between DEN and DEN-FBRP groups at the time points of weeks 4, 8, 12, and 15 (Figures 4B and 4C). The liver index of rats in the DEN injury model was significantly higher than that in normal and normal-FBRP groups (both $p < 0.001$, Figure 4C); however, the administration of FBRP dramatically reduced the liver index of the DEN rats, which were significantly higher than the normal rats at the time point of week 18 in Figure 4C ($p < 0.001$).

FBRP Ameliorates Histological Changes in DEN-Induced HCC Rats

In accordance with the above gross anatomy observation, histologically, we found normal organization of hepatic lobules, normal hepatocytes, and sinusoidal architecture without fibroplasia and inflammatory cell infiltration, but just the scattered foci of fatty degeneration observed in normal and normal-FBRP rats (marked with green arrows in Figure 5A). In contrast, DEN injury by 12 weeks displayed obvious microscopic fibrosis and cirrhosis, as well as hemorrhagic necrosis with foci of inflammatory cells around fibrosis tissue (marked with red arrows in Figure 5A). Subsequent to hepatic fibrosis, the incidence of tumors markedly increased. All rats in the DEN-induced model group developed HCC by week 18. The white nodules observed on the surface of the livers were histologically confirmed to be HCC, the cells of which had clear, eosinophilic or hyperbasophilic cytoplasm, and all had enlarged and hyperchromatic nuclei (marked with blue arrows in Figure 5A). With the administration of FBRP, the histological patterns of the livers showed a

FBRP Suppresses Proliferation and Induces Cell Cycle Arrest of HCC Cells

To confirm the cytotoxicity of FBRP on the HCC cell line, we performed a Cell Counting Kit-8 (CCK-8) assay and the results showed that the treatment of 5 and 10 μg/mL FBRP both suppressed the proliferation of Huh7 cells significantly (all $p < 0.05$, Figure 6A). Next, the cell cycle assay was evaluated to investigate whether FBRP has inhibitory effects on the HCC cell line. The results showed that FBRP effectively induced cycle arrest of Huh7 cells in the G_1 phase (all $p < 0.05$, Figures 6B–6E).

FBRP Inhibits PI3K/AKT/NF-κB Signaling in DEN-Induced HCC Rats In Vivo and HCC Cells In Vitro

We first performed quantitative PCR analysis and an enzyme-linked immunosorbent assay (ELISA) to examine the expression of the FBRP putative targets ABCC2, CYP2B6, CYP2C19, CYP2D6, CYP3A4, CYP3A5, and CYP3A7, which are also the targets of sorafenib, in the normal control, DEN, and DEN-FBRP groups. As
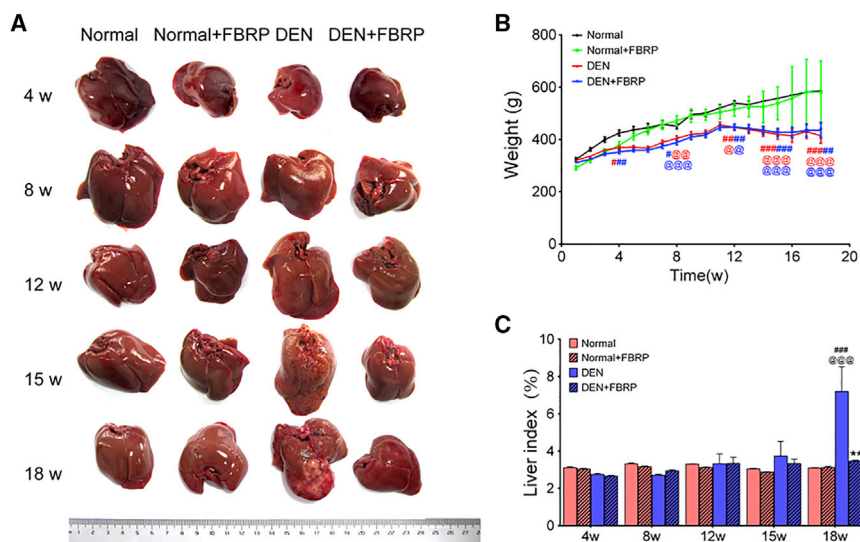
Figure 4. Effects of FBRP on the Generation of Neoplastic Lesions and Associated Fibrosis on DEN-Induced HCC Rats, as well as Its Influence on Body Weight and the Liver Index

(A) Generation of neoplastic lesions and associated fibrosis of rats in different groups. (B) Body weight of rats in different groups. (C) Liver index of rats in different groups. Data are expressed as the mean ± SD. #$p < 0.05$, ##$p < 0.01$, ###$p < 0.001$, comparison with the normal group; @$p < 0.05$, @@$p < 0.01$, @@@$p < 0.001$, comparison with the normal+FBRP group; *$p < 0.05$, **$p < 0.01$, ***$p < 0.001$, comparison with the DEN group.

shown in Figure S1A, the elevated expression levels of ABCC2 mRNA in DEN groups were observed from week 12 to week 18, which were effectively reduced by treatment with FBRP (all $p < 0.05$). Similarly, the serum levels of CYP3A4 and CYP2B6 in DEN rats were higher than those in FBRP-treated DEN rats from week 12 to week 18 (all $p < 0.05$, Figures S1B and S1C). In weeks 12, 15, and 18, the serum levels of CYP2D6 (in week 15, all $p < 0.05$, Figure S1D), CYP3A5 (in weeks 12 and 18, all $p < 0.05$, Figure S1E), CYP3A7 (in weeks 12 and 18, all $p < 0.01$, Figure S1F), and CYP2C19 (in weeks 12 and 18, all $p < 0.05$, Figure S1G) were also increased by DEN injury, but effectively suppressed by the treatment of FBRP.

To determine whether PI3K/AKT/NF-κB signaling was the principal target of FBRP against DEN-induced HCC, we performed western blot analysis to detect the expression levels of phosphorylated (p-)PI3K, p-AKT, total IKκB, p-IKκB, total NF-κB, and p-NF-κB proteins in DEN-injured liver tissues. As a result, we observed an increase in the expression of p-PI3K, p-AKT, p-IKκB, and p-NF-κB, as well as the ratios of p-IKκB/total IKκB and p-NF-κB/total NF-κB, in HCC model rats from week 12 to week 18, suggesting the activation of PI3K/AKT/NF-κB signaling induced by DEN administration. Following the treatment of FBRP, DEN-induced PI3K/AKT/NF-κB signaling activation was significantly suppressed (all $p < 0.05$, Figures 7A–7I).

Consistently, our immunofluorescence assay showed marked NF-κB (p65) translocation into the nucleus after DEN administration ($p < 0.05$, Figures 8A–8C). In contrast, the nuclear import of NF-κB (p65) was significantly decreased in liver tissues of FBRP-treated rats ($p < 0.05$, Figures 8A–8C). No significant changes in the intensity of immunofluorescence signals showing NF-κB (p65) translocation into the nucleus were observed between normal control and normal-FBRP groups. These findings suggest that FBRP may affect NF-κB activation in DEN-induced HCC rats.

In addition, we performed immunohistochemistry and western blot analyses to examine the subcellular localization and the expression levels of the downstream factors in PI3K/AKT/NF-κB signaling, including CCND1, CCNE1, CDK2, and CDK4. As shown in Figures 9A–9E, immunohistochemistry indicated the stronger cytoplasm and/or nuclear positive staining of the cell proliferation factor PCNA protein, as well as CCND1, CCNE1, CDK2, and CDK4 proteins in DEN injury liver tissues, which were effectively reduced by the treatment with FBRP. Statistically, the expression levels of the five proteins in the DEN-induced HCC model group were significantly higher than those in normal control and normal-FBRP groups, whereas FBRP treatment suppressed this enhancement (all $p < 0.05$, Figures 9A–9E), which were also in line with the findings of western blot analysis (all $p < 0.05$, Figures 7A and 7J–7M).

Moreover, we explored the effects of FBRP on PI3K/AKT/NF-κB signaling in the HCC cell line Huh7. The results showed that the expressions of p-PI3K, p-AKT, p-IKκB, and p-NF-κB, as well as the ratios of p-IKκB/total IKκB and p-NF-κB/total NF-κB, were significantly decreased by FBRP (all $p < 0.05$, Figure 10A–10F). We also found that there were obvious changes in the expression of the downstream factors in the PI3K/AKT/NF-κB signaling, including CCND1, CCNE1, CDK2, and CDK4 proteins (all $p < 0.05$, Figures 10G–10K).

To further verify the possible involvement of PI3K/AKT/NF-κB signaling in the anti-cancer efficacy of FBRP, the PI3K inhibitor LY294002 was applied. As shown in Figure 10, LY294002 treatment significantly decreased the phosphorylated levels of PI3K, AKT, IKκB, and NF-κB, as well as the ratios of p-IKκB/total IKκB and p-NF-κB/total NF-κB. Notably, the co-treatment of FBRP with the PI3K inhibitor LY294002 exhibited an additive inhibitory effect on PI3K/AKT/NF-κB signaling activation (all $p < 0.05$, Figure 10).

DISCUSSION

Sorafenib was approved by FDA and is usually used as a standard regimen in the treatment of HCC. Unfortunately, recent clinical evidence has shown that an increasing number of HCC patients appear to be resistant to sorafenib.[26] There have been more than 50 target drugs in clinical trials for the treatment of HCC; however, none of
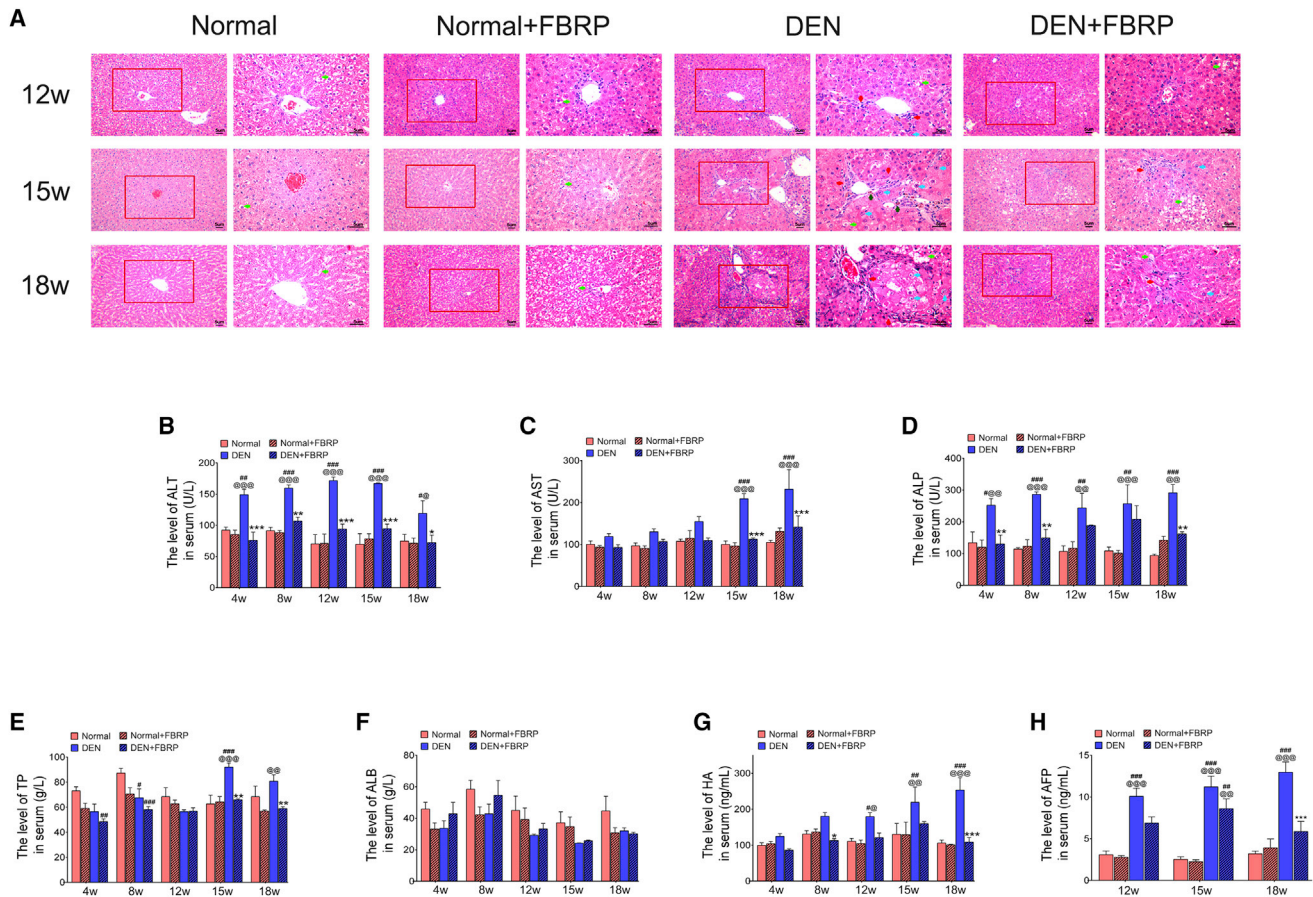
Figure 5. Effects of FBRP on the Histological Changes of Liver in DEN-Induced HCC Rats, as well as Its Influence on the Liver Function-Related Serum Parameters (ALT, AST, ALP, TP, ALB), as well as Fibrosis (HA)- and Tumor-Related Serum Markers (AFP)

(A) Effects of FBRP on the histological changes of liver in DEN-induced HCC rats. Red boxes represent the area with typical pathological changes. Scale bars represent 5 μm. (B–H) Serum levels of ALT (B), AST (C), ALP (D), TP (E), ALB (F), HA (G), and AFP (H) in different groups. Data are expressed as the mean ± SD. $^{\#}p < 0.05$, $^{\#\#}p < 0.01$, $^{\#\#\#}p < 0.001$, comparison with the normal group; $^{@}p < 0.05$, $^{@@}p < 0.01$, $^{@@@}p < 0.001$, comparison with the normal+FBRP group; $^{*}p < 0.05$, $^{**}p < 0.01$, $^{***}p < 0.001$, comparison with the DEN group.

them has been demonstrated to be superior to sorafenib.[27] Therefore, the discovery of novel and effective anti-HCC drugs may be a significant challenge in drug development. Drug repositioning refers to the identification and the development of new usage for existing drugs to reduce the overall cost and shorten the time required to bring new drugs into commerce. In the current study, we suggest the integrated network-based computational and experimental workflow for discovering potential therapeutic effects of the clinically approved anti-fibrosis formula FBRP in HCC treatment. In our results, seven FBRP putative targets were also the targets of several FDA-approved anti-HCC drugs, such as sorafenib and regorafenib, and FBRP putative targets were significantly enriched in various biological processes and pathways involved in the progression of inflammation-fibrosis-tumorigenesis transformation, implying the potentials of FBRP to treat HCC. Then, both key network target identification and functional module analysis demonstrated that the PI3K/AKT/NF-κB signaling-mediated cell proliferation pathway might be the candidate

network target of FBRP reversing the hepatic fibrosis-cirrhosis-cancer axis. Experimentally, we validated that FBRP could inhibit the generation of neoplastic lesions, improve associated fibrosis, prolong survival, ameliorate histological changes, and suppress liver function-related serum parameters, fibrosis, and tumor-related serum markers of DEN-induced HCC rats *in vivo*, as well as inhibit the proliferation and induce cell cycle arrest of HCC cells *in vitro*. Moreover, both western blot and immunofluorescence analyses demonstrated the inhibitory effects of FBRP treatment on the activation of PI3K/AKT/NF-κB signaling, subsequently leading to the reduced expression and positive immunostaining of the downstream molecules, including CCND1, CCNE1, PCNA, CDK2, and CDK4 proteins. Consistently, the co-treatment of FBRP with PI3K inhibitor LY294002 exhibited an additive inhibitory effect on PI3K/AKT/NF-κB signaling activation. The above findings suggest that FBRP may be applied for treating HCC, which is developed by the hepatic fibrosis-cirrhosis-cancer axis. Compared with previous studies, the
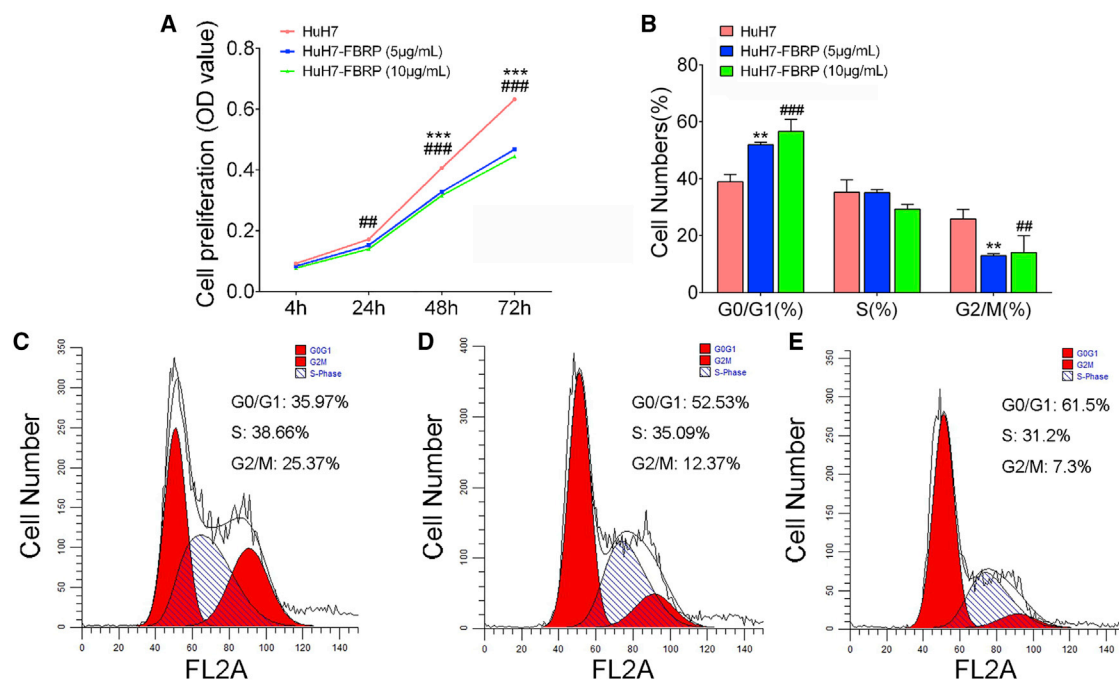
Figure 6. Effects of FBRP on Cell Proliferation and Cell Cycle of the HCC Cell Line Huh7

(A) Optical density (OD) values of different groups detected by the CCK-8 assay. (B) Histograms show the proportions of cell cycle distribution in the G_1, S, and G_2/M phase of Huh7 cells in different groups. (C) Flow cytometry analysis of the cell cycle distribution of Huh7 cells without FBRP treatment. (D) Flow cytometry analysis of the cell cycle distribution of Huh7 cells treated with 5μg/mL FBRP. (E) Flow cytometry analysis of the cell cycle distribution of Huh7 cells treated with 10μg/mL FBRP. *$p < 0.05$, **$p < 0.01$, ***$p < 0.001$, Huh7-FBRP (5 μg/mL) group comparison with the Huh7 group; #$p < 0.05$, ##$p < 0.01$, ###$p < 0.001$, Huh7-FBRP (10 μg/mL) group comparison with the Huh7 group.

current study is characterized by the integration of network-based computational and experimental methods for the discovery of novel therapeutic effects of FBRP and a more comprehensive understanding of its underlying mechanism.

To increase the success rate of clinical translation, we used the DEN rat model specifically to simulate the aggressive progression from hepatic fibrosis, cirrhosis, and HCC to validate our prediction. All surviving rats of the DEN model group appeared to have HCC at the end of the experiment. From the general and pathological observation on the DEN-injury liver tissues, our DEN-induced HCC model developed three stages, including the inflammation stage, the fibrosis stage, and the HCC stage, and the three stages with mixer features were shown from week 12 to week 18. The association between inflammation and cancer was first proposed by the German pathologist Rudolf Virchow in the mid-19th century.[28] From then on, the underlying molecular mechanisms of the inflammation-fibrosis-cancer axis gradually attracted the attention of scholars. In line with our observation, recent studies have indicated that inflammatory processes may trigger the molecular and cellular events that subsequently lead to hepatic fibrosis and ultimately promote liver cancer generation.[29] When treated with FBRP, the general and histological changes of liver tissues, as well as levels of liver function-related serum parameters and fibrosis and tumor-related serum markers, in our hepatocarcinogenic rat model using a DEN

diet were all significantly reversed, suggesting that FBRP may effectively inhibit the generation of HCC and preneoplastic lesions. Especially, its suppression of preneoplastic lesions may also imply a direct anti-carcinogenesis effect of FBRP.

To further unveil the potential mechanisms of FBRP against HCC, our network-based investigation identified a list of candidate FBRP targets that might play a crucial role in reversing the hepatic fibrosis-cirrhosis-cancer axis, and we divided their enriched cancer-related pathways into three modules: carcinogenesis, immune regulation and inflammation, and metabolism pathways. Among them, PI3K/AKT/NF-κB signaling was the top one involved by candidate FBRP targets acting on HCC. Consistently, accumulating studies have indicated that PI3K/AKT/NF-κB signaling is involved in the regulation of tumor cell growth, proliferation, tumor migration, and invasion, as well as metabolism.[23] The activation of this signaling has been proven in multiple types of human cancers.[25] From our *in vivo* experiments, the administration of DEN for 12 weeks led to the increased activation and expression of p-PI3K, p-AKT, p-IKκB, and p-NF-κB, and a further increase was observed during the extended DEN treatment period to 18 weeks, suggesting a direct causal association between the duration of DEN treatment and PI3K/AKT/NF-κB signaling activation. Thus, we indicated that the activation of PI3K/AKT/NF-κB signaling by DEN injury may be time-dependent and may closely relate to
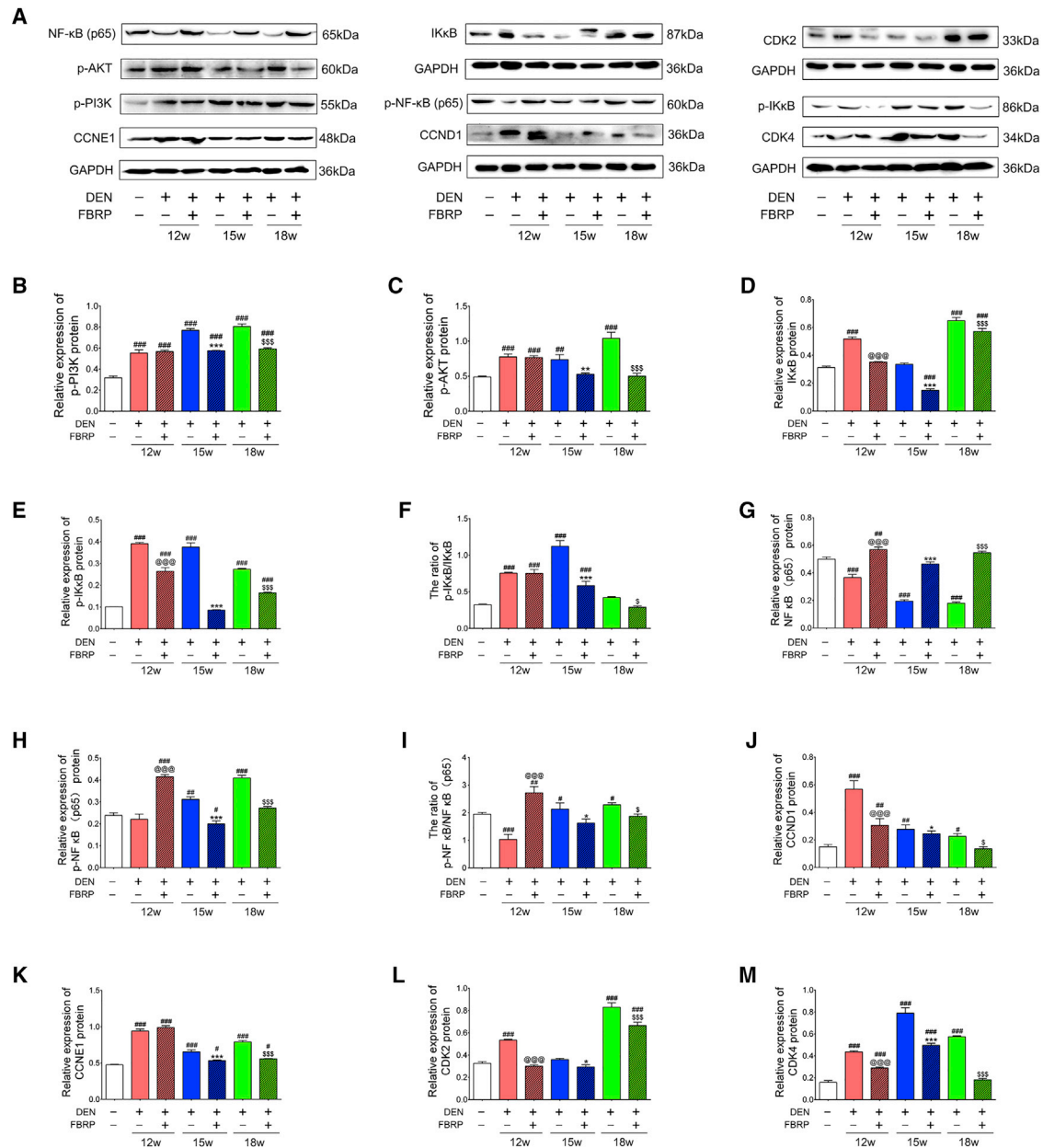
Figure 7. Effects of FBRP on Expression Levels of Candidate Targets Involved in PI3K/AKT/NF-κB Signaling in Liver Tissues of DEN-Induced HCC Rats

(A) Western blots of the candidate targets of FBRP against HCC involved in PI3K/AKT/NF-κB signaling. (B–M) Relative protein expression levels of (B) p-PI3K, (C) p-AKT, (D) IKκB, (E) p-IKκB, (F) the ratio of p-IKκB to IKκB, (G) NF-κB (p65), (H) p-NF-κB (p65), (I) the ratio of NF-κB (p65) to p-NF-κB (p65), (J) CCND1, (K) CCNE1, (L) CDK2, and (M) CDK4 in different groups are shown. Data are expressed as the mean ± SD. $^{\#}p < 0.05$, $^{\#\#}p < 0.01$, $^{\#\#\#}p < 0.001$, comparison with the normal group; $^{@}p < 0.05$, $^{@@}p < 0.01$, $^{@@@}p < 0.001$, comparison with the DEN-12w group; $^{*}p < 0.05$, $^{**}p < 0.01$, $^{***}p < 0.001$, comparison with the DEN-15w group; $^{\$}p < 0.05$, $^{\$\$}p < 0.01$, $^{\$\$\$}p < 0.001$, comparison with the DEN-18w group.

HCC progression. In contrast, for the concomitant treatment with FBRP, the expression levels of p-PI3K, p-AKT, p-IKκB, and p-NF-κB proteins, the ratio of phosphorylation to TPs, and the translocation into nuclear of NF-κB were all decreased markedly. Moreover, the western blot analysis and immunohistochemistry were also employed to verify the effects of FBRP to modulate the

downstream molecules of PI3K/AKT/NF-κB signaling. Since recent studies have revealed that cell proliferation and cell cycle arrest in the G_1 phase may be mainly mediated by the downregulation of CCND1, CCNE1, CDK2, and CDK4 proteins,[30,31] herein the cell proliferation and cell cycle of HCC cell line Huh7 were examined and the results showed that FBRP suppressed the cell proliferation
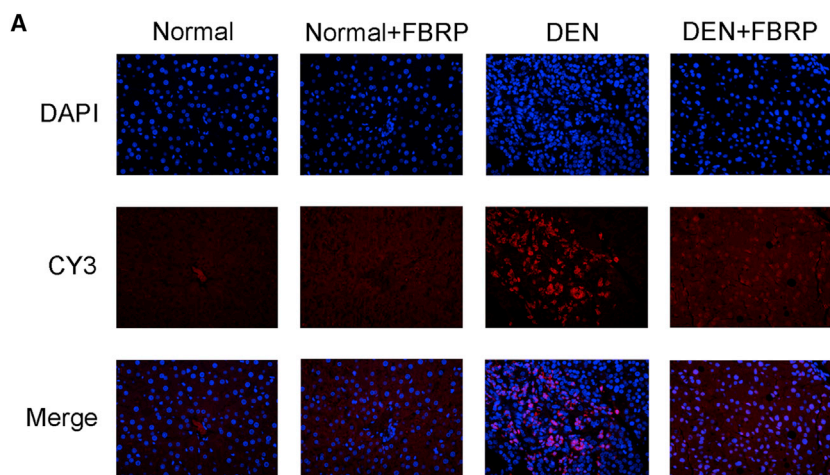
A

B

C

Figure 8. Expression and Distribution of NF-κB (p65) Protein in Liver Tissues of DEN-Induced HCC Rats and Their Quantification Results

(A) Expression and distribution of NF-κB (p65) protein in liver tissues of DEN-induced HCC rats with or without FBRP treatment. Original magnification, ×400. (B) IOD value of NF-κB (p65) in nuclear in liver tissues of DEN-induced HCC rats with or without FBRP treatment. (C) Ratio of the number of cells with NF-κB (p65) nuclei translocation to the total number of cells in liver tissues of DEN-induced HCC rats with or without FBRP treatment. Data are expressed as the mean ± SD. #p < 0.05, ##p < 0.01, ###p < 0.001, comparison with the normal group; @p < 0.05, @@p < 0.01, @@@p < 0.001, comparison with the normal+FBRP group; *p < 0.05, **p < 0.01, ***p < 0.001, comparison with the DEN group.
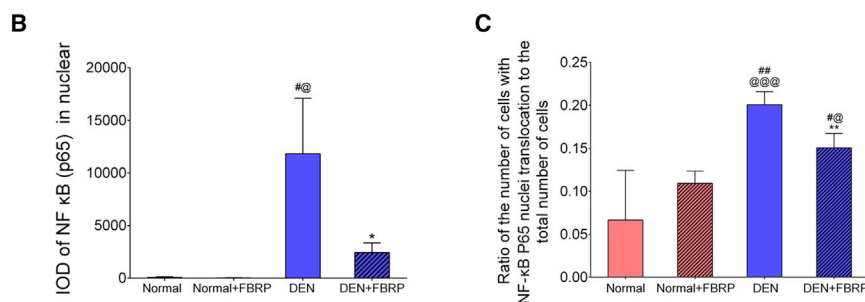
and induced cycle arrest of HCC cells in the G_1 phase, which were validated by the alteration of CCND1, CCNE1, CDK2, and CDK4 proteins. Next, we verified that the co-treatment of FBRP with the PI3K inhibitor LY294002 exhibited the additive inhibitory effect on PI3K/AKT/NF-κB signaling activation, suggesting that the anti-HCC efficacy of FBRP may be mediated, at least in part, by PI3K/AKT/NF-κB signaling.

In conclusion, our data showed the potentials of FBRP in hepatic fibrosis microenvironment regulation and tumor prevention, suggesting that FBRP may be a promising candidate drug for reduction of fibrogenesis and prevention of HCC. We also provided an integrated network-based strategy for unveiling that FBRP may block PI3K/AKT/NF-κB activation, further highlighting the multi-target anti-HCC effect of this prescription.

MATERIALS AND METHODS

Ethics Statement

All experimental protocols were approved by the Research Ethics Committee of the Institute of Chinese Materia Medica, China Academy of Chinese Medical Sciences, and the 302 Military Hospital, Beijing, China (no. 2016003D). Animal experiments were carried out in accordance with the guidelines and regulations for the care and use of laboratory animals of the Center for Laboratory Animal Care, China Academy of Chinese Medical Sciences, Beijing, China.

Network-Based Drug Repositioning Analysis

Prediction of FBRP Putative Targets

The chemical components containing FBRP were collected from a TCM-related database, ETCM (http://www.nrc.ac.cn:9090/ETCM/, 2018), constructed by our research group.[19] ETCM estimated drug-likeness of each chemical component by calculating the quantitative estimate of drug-likeness (QED) score based on models in the Pipeline Pilot ADMET collection, such as aqueous solubility, blood-brain barrier penetration, CYP450 2D6 inhibition, hepatotoxicity, human intestinal absorption, and plasma protein binding, and it classified chemical components into three groups according to their QED scores, good (QED > 0.67), moderate (0.49 ≤ QED ≤ 0.67), and weak (QED < 0.49) drug-likeness. In this study, we chose the chemical components with moderate to good drug-likeness as the candidate bioactive components of FBRP for the following target predictions.

On the basis of structural and functional similarity of drugs, the putative target hits for the candidate bioactive components of FBRP were predicted using MedChem Studio (version 3.0; Simulations Plus, Lancaster, CA, USA, 2012). The component-putative target pairs with similarity scores higher than 0.90 (high similarity) were selected for further investigation.

Collection of Hepatic Fibrosis, Cirrhosis, and HCC-Related Genes

Known therapeutic targets of hepatic fibrosis, cirrhosis, and HCC were collected from the DrugBank database[32] (http://www.drugbank.ca/, version: 5.0). The drug-target interactions in which drugs are approved by FDA for the treatment of hepatic fibrosis, cirrhosis, and HCC and the targets for human genes/proteins were enrolled. In addition, the hepatic fibrosis-, cirrhosis-, and HCC-related genes were also collected from the Library of
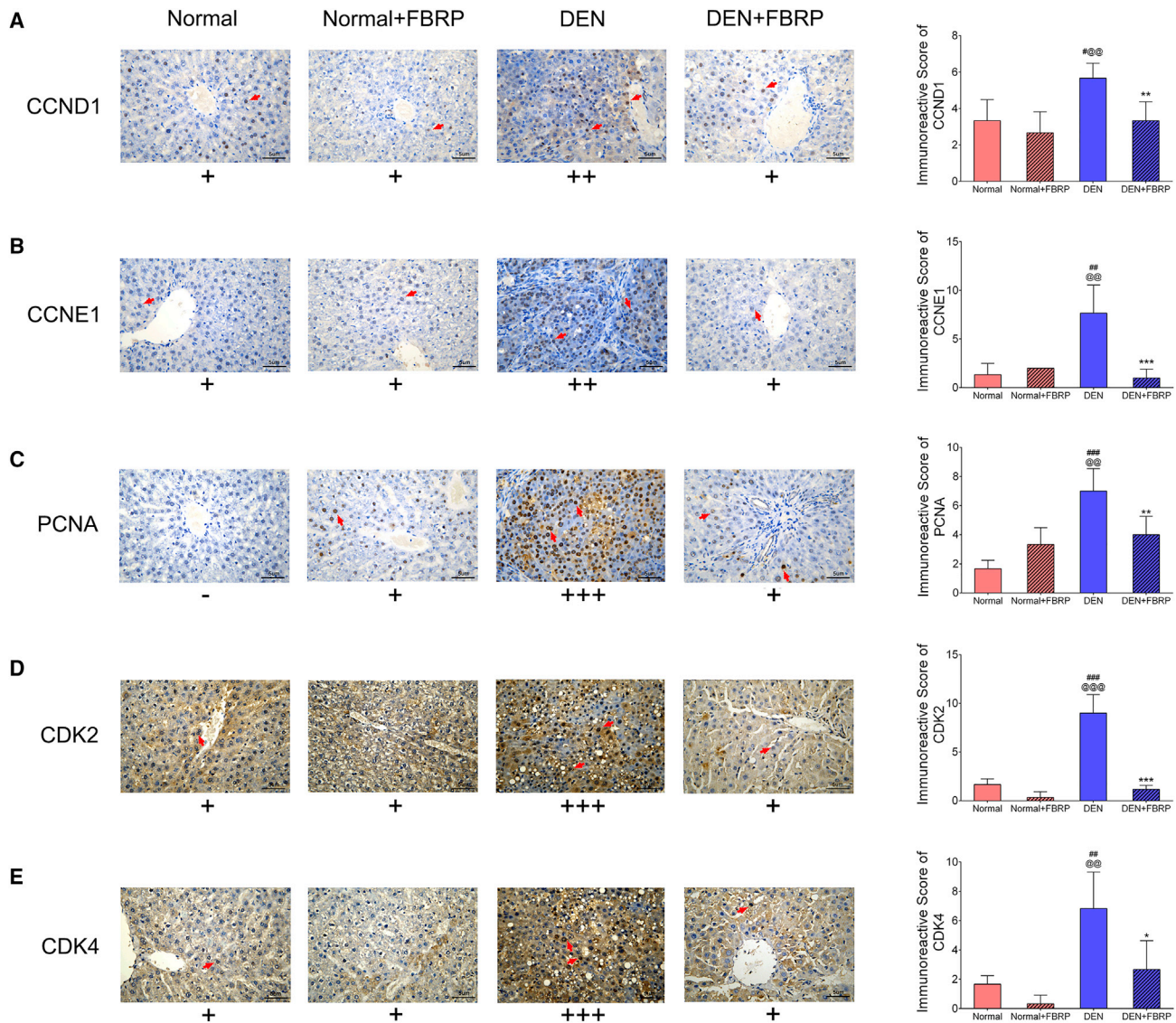
Figure 9. The Immunohistochemistry Analysis of the Effects of FBRP on the Subcellular Localization and Expression Levels of the Downstream Factors in PI3K/AKT/NF-κB Signaling in Liver Tissues of DEN-Induced HCC Rats and Their Quantification Results

(A–E) Effects of FBRP on the expression of (A) CCND1, (B) CCNE1, (C) PCNA, (D) CDK2, and (E) CDK4 in the liver tissues of DEN-induced HCC rats examined by immunohistochemistry. Original magnification, ×400. Data are expressed as the mean ± SD. $^{\#}p < 0.05$, $^{\#\#}p < 0.01$, $^{\#\#\#}p < 0.001$, comparison with the normal group; $^{@}p < 0.05$, $^{@@}p < 0.01$, $^{@@@}p < 0.001$, comparison with the normal+FBRP group; $^{*}p < 0.05$, $^{**}p < 0.01$, $^{***}p < 0.001$, comparison with the DEN group.

Molecular Associations (LOMA)[33] which holds approximately 1,260 confirmed molecular associations for various liver diseases such as HCC, hepatic fibrosis, cirrhosis, and nonalcoholic steatohepatitis (NASH)/fatty liver disease. The list of hepatic fibrosis-, cirrhosis-, and HCC-related genes is provided in Table S5.

Network Construction and Analysis

The disease gene-drug target network was constructed using links between hepatic fibrosis-cancer axis-related genes and FBRP putative targets according to the public database STRING (Search Tool for Known and Predicted Protein-Protein Interactions, version 10.0, http://string-db.org/). The gene-gene interactions with combined scores higher than the median value of all combined scores were selected in this study. To screen the network target with the topological importance of in the networks, we calculated four topological features, including the node degree, betweenness, closeness, and k-coreness according to our previous studies.[33,34] Modularity analysis was performed to divide nodes, which are highly interconnected within the network, into different functional modules using the Markov clustering algorithm. The networks were visualized by Navigator software (version 2.2.1).
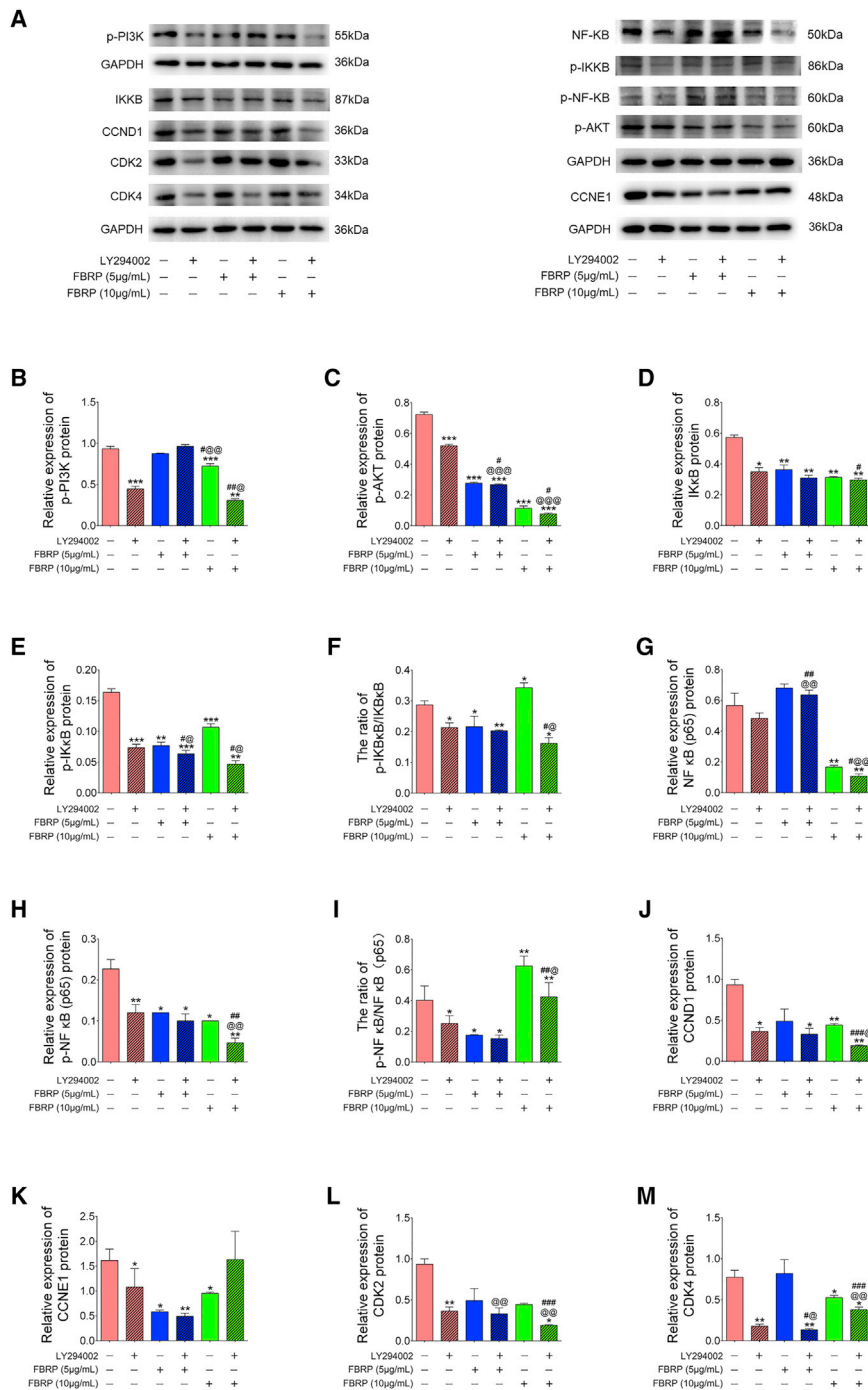
Figure 10. Effects of FBRP on Expression Levels of Candidate Targets Involved in PI3K/AKT/NF-κB Signaling in the HCC Cell Line Huh7

(A) Western blots of the candidate targets of FBRP against HCC involved in PI3K/AKT/NF-κB signaling in different groups. (B–M) Relative protein expression levels of (B) p-PI3K, (C) p-AKT, (D) IKκB, (E) p-IKκB, (F) the ratio of p-IKκB to IKκB, (G) NF-κB (p65), (H) p-NF-κB (p65), (I) the ratio of NF-κB (p65) to p-NF-κB (p65), (J) CCND1, (K) CCNE1, (L) CDK2, and (M) CDK4 in different groups are shown. Data are expressed as the mean ± SD. *p < 0.05, **p < 0.01, ***p < 0.001, comparison with the Huh7 group; #p < 0.05, ##p < 0.01, ###p < 0.001, comparison with the Huh7-FBRP treatment group; @p < 0.05, @@p < 0.01, @@@p < 0.001, comparison with the Huh7-LY294002 group.

KEGG pathways with p values <0.05 (corrected using the Bonferroni method) were selected.

Experimental Validations
Animals and Treatment

Male Sprague-Dawley (SD) rats (n = 80, 240–260 g in weight) were purchased from Guangdong Medical Laboratory Animal Center (production license no. SCXK 2013-0002, Guangzhou, China). All rats were kept under specific pathogen-free conditions, with a constant temperature of 24°C ± 1°C in a 12-h light/12-h dark cycle room and *ad libitum* water and food access. Prior to the experiments, the rats were allowed a 1-week acclimatization period.

A total of 80 SD rats were randomly divided into four groups: normal control (n = 15), FBRP (n = 15), DEN model (n = 25), and DEN-FBRP (n = 25) groups. Normal control rats were fed a normal diet. FBRP groups received daily oral administration of 1 g/kg FBRP and with normal drinking water. DEN model and DEN-FBRP group rats were given 0.01% DEN (catalog no. N0756, Sigma-Aldrich, St. Louis, MO, USA) *ad libitum* in their drinking water for a period of 18 weeks. Rats in the DEN-FBRP group received daily oral administration of 1 g/kg FBRP (catalog no. Z19991011, Furui Medical Science, Beijing, China) from the day of DEN modeling until 18 weeks. The dosage selection for FBRP (1 g/kg) was twice the daily dosage of hepatic fibrosis patients in clinics, which has been proven to exert the most prominent therapeutic efficacy in patients with hepatic fibrosis.[34]

Body weight of the rats was measured once every week throughout the study. To monitor the progress of stepwise hepatocarcinogenesis, a

Pathway Enrichment Analyses

Pathway enrichment analysis of FBRP candidate targets against HCC was performed using the Database for Annotation, Visualization and Integrated Discovery (DAVID, http://david.abcc ncifcrf.gov/home.jsp, version 6.7) based on the data obtained from the FTP service of KEGG (http://www.genome.jp/kegg/, last updated on October 16, 2012). Only

time-serial sera set, including five rats from the DEN and DEN-FBRP groups and three rats from control group, was sacrificed at 4, 8, 12, 15, and 18 weeks. At the time of sacrifice, tumors were counted and measured. The liver index, the ratio of liver weight to body weight, is a commonly used toxicological parameter. The increased liver index indicates edema, hyperemia, or hypertrophy of the liver; conversely, it indicates liver atrophy or other degenerative changes. Then, the liver was then sectioned and fixed in 10% formalin. The remaining portions of the liver were snap-frozen and stored at −80°C until use.

Detection of Biochemical Indicators and Fibrosis-Related Index

Blood samples were collected via the orbital venous system. Serum levels of ALT, AST, ALP, TP, and ALB, as well as the liver fibrosis marker HA, were all tested using an automatic analyzer (AU5831; Beckman Coulter, CA, USA). In addition, serum levels of AFP and the FBRP putative targets CYP2B6, CYP2C19, CYP2D6, CYP3A4, CYP3A5 and CYP3A7, which are also the targets of sorafenib, were measured using ELISA kits according to the manufacturer's instruction. Detailed information of all ELISA kits is provided in Table S6.

Histopathological Evaluation

Extracted rat livers were fixed in 10% formalin. Following routine procedures, 3-μm-thick sections were obtained from the resulting paraffin blocks. After deparaffinization and rehydration, sections were stained with hematoxylin and eosin. All sections were examined under a light microscope (ML31, Mshot, Guangzhou, China).

Immunohistochemical Staining

Immunohistochemical staining was conducted using an UltraSensitive SP (mouse/rabbit) immunohistochemistry (IHC) kit (catalog no. KIT-0305; MX Biotechnologies, Fuzhou, China), which contained endogenous peroxidase blocking solution, serum, secondary antibody, streptavidin-peroxidase, and diaminobenzidine (DAB) substrate-chromogen. The rat liver tissue sections were incubated overnight at 4°C with cyclin D1 (dilution 1:400, catalog no. 2978T, Cell Signaling Technology, MA, USA), cyclin E1 (dilution 1:300, catalog no. Ab33911, Abcam, MA, USA), CDK2 (dilution 1:1,000, catalog no. 10122-1-AP, Proteintech, IL, USA), CDK4 (dilution 1:1,000, catalog no. 11026-1-AP, Proteintech, IL, USA), and PCNA (dilution 1:800, catalog no. Sc-56, Santa Cruz Biotechnology, CA, USA) antibodies. Following washing, the sections were incubated with an avidin-conjugated secondary antibody contained in an UltraSensitive SP (mouse/rabbit) IHC kit (catalog no. KIT-0305; MX Biotechnologies, Fuzhou, China) for 30 min at room temperature. Streptavidin-peroxidase-labeled polymer (50 μL for 15 min at room temperature) and substrate-chromogen (100 μL for 2 min at room temperature) were used to observe the staining of the target protein. For negative controls, the primary antibody was omitted in each IHC run.

The intensity of dyeing score was determined according to the protocol in Handala et al.[35] Given the heterogeneity of the staining of the proteins, tumor specimens were scored in a semiquantitative manner.

The percentages were grouped as follows: 0 (0%), 1 (1%–10%), 2 (11%–50%), and 3 (>50%). The staining intensity was categorized as follows: 0, negative; 1, weak; 2, moderate; and 3, strong. A final score was obtained for each case by the multiply of the percentages and the intensity scores.

Immunofluorescence Assay

Formalin-fixed paraffin sections of rat liver (3-μm thickness) were deparaffinized before antigen retrieval. Endogenous peroxidase was blocked by incubating in 3% H_2O_2 in methanol for 15 min. The liver slices were blocked with phosphate-buffered saline (PBS) containing 0.05% Triton X-100 (EZ1609D315, BioFroxx) and 10% goat serum and then incubated with a 1:100 dilution of NF-κB antibody (catalog no. GB11034, Servicebio, Wuhan, China) at 4°C overnight. The slices were washed and incubated with Cy3-conjugated goat anti-mouse IgG (H+L) (catalog no. GB21301, Servicebio, Wuhan, China) as appropriate for 45 min at room temperature, washed extensively, and mounted with ProLong Gold antifade reagent (catalog no. P36941, Thermo Fisher Scientific, CA, USA), Nuclei were stained with 4′,6-diamidino-2-phenylindole (DAPI; 1:1,000; Invitrogen) for 2 min. Immunofluorescence was visualized under a fluorescence microscope (Nikon Eclipse C1, Nikon, Japan). The immunofluorescence results of NF-KB were quantified by ImageJ (version 1.52e, National Institutes of Health, USA; http://imagej.nih.gov/ij). Two images of each field were analyzed. The DAPI staining image was converted to a DAPI staining mask, and the NF-κB staining image was converted to a specific staining mask by implementing Huang and Wang's[34] fuzzy thresholding method. A third mask corresponding to the nuclei of the immunostained cells was created using the "Image Calculator" command and the "AND" operator. Finally, NF-κB transfer to the nuclei was quantified using the "Analyze Particles" tool.[35] The integrated optical density (IOD) value of NF-κB in nuclei was examined, and the ratio of the number of cells with NF-κB (p65) nuclei translocation to the total number of cells was calculated to represent the level of NF-κB nuclear translocation.

Culture and treatment of HCC cell line Huh7

The human HCC cell line Huh7 (catalog no. TCHu182, Cell Bank of Typical Culture Preservation Committee of Chinese Academy of Sciences, Shanghai, China) was used for *in vitro* experimental validation. Huh7 cells were maintained in Dulbecco's modified Eagle's medium (DMEM, catalog no. SH30022-01B, Thermo Scientific/HyClone, USA) supplemented with 10% FBS, 100 IU/mL penicillin, 100 mg/mL streptomycin, and 2 mmol/L glutamine, supplemented with 100 U/mL penicillin, 80 U/mL streptomycin, 2 mM glutamine, and 10% fetal bovine serum (FBS) in a humidified 5% CO_2 incubator at 37°C.

For drug administration, Huh7 cells were divided into the following groups: (1) control group (no treatment), (2) FBRP treatment group with a low dosage of FBRP (cells were treated with 5.0 μg/mL FBRP for 24 h), and (3) FBRP treatment group with high dosage of FBRP (cells were treated with 10.0 μg/mL FBRP for 24 h).

Cell Proliferation Assay

Cell viability of Huh7 cells in different groups was detected with a CCK-8 assay (catalog no. C0039, Beyotime Biotechnology, Jiangsu, China) according to the protocol described in our previous studies.[36]

Cell Cycle Assay

Huh7 cells were seeded into six-well plates and reached approximately 70%–80% confluence. Cells were collected and fixed in 70% ethanol at $-20°C$ overnight. After resuspending the cells, 20 µg/mL PBS, 200 µg/mL RNaseA, and 0.1% Triton X-100 were added into the solution. Then, the cell suspension was incubated in the dark for 30 min at $4°C$. The cell cycle assay was analyzed by flow cytometry (BD FACSCalibur, BD Biosciences, USA). Each test was conducted three times.

Western Blot Analysis

Proteins were extracted by a mixture of radioimmunoprecipitation assay (RIPA; catalog no. P0013B, Beyotime Biotechnology, Shanghai, China) lysis buffer and protease inhibitor (100 mM, catalog no. ST506, Beyotime Biotechnology, Shanghai, China) at a ratio of 49:1 for 1 h. Then, supernatant liquid was obtained after centrifuging at 12,000 rpm for 15 min. Protein quantification was performed using bicinchoninic acid (BCA; catalog no. 23227, Thermo Scientific, US) and separated by 10% sodium dodecyl sulfate polyacrylamide gel electrophoresis (SDS-PAGE) and transferred to nitrocellulose membranes. After blocking with 10% skim milk (catalog no. 7198868, Difco/Becton Dickinson, US), the membrane was incubated with the corresponding antibodies at $4°C$ overnight. The detailed information on these antibodies is as follows: p-PI3K (catalog no. 4249, Cell Signaling Technology, MA, USA), p-AKT (catalog no. 4060, Cell Signaling Technology, MA, USA), IKκB (catalog no. 8943, Cell Signaling Technology, MA, USA), p-IKκB (catalog no. YP0637, ImmunoWay, TX, USA), NF-κB (p65) (catalog no. YP0191, ImmunoWay, TX, USA), p-NF-κB (p65) (catalog no. 3033, Cell Signaling Technology, MA, USA), CCND1 (catalog no. 2978, Cell Signaling Technology, MA, USA), CCNE1 (catalog no. 20808, Cell Signaling Technology, MA, USA), CDK2 (catalog no. 10122-1-AP, Proteintech, IL, USA), CDK4 (catalog no. 11026-1-AP, Proteintech, IL, USA), and GAPDH (catalog no. 2118, Cell Signaling Technology, MA, USA). In addition, the membrane was incubated with horseradish peroxidase (HRP)-conjugated secondary antibody (catalog no. SA00001-2, Proteintech, IL, USA) for a further 2 h after washing three times with Tris-buffered saline with Tween 20 (TBST). Finally, the immunoreactive protein bands were detected by a chemiluminescence imaging analysis system (5200, Tanon, China). The relative density of protein expression was quantified by ImageJ software (NIH).

Quantitative PCR Analysis

To examine the expression of the FBRP putative targets, ABCC2, which is also the target of sorafenib, in the normal control, the normal-FBRP groups, DEN and DEN-FBRP groups, quantitative PCR analysis for ABCC2 mRNA was performed according to our previous studies.[34] ACTB was used as an internal control for ABCC2

mRNA expression normalization and quantification. Quantitative PCR analysis and data collection were performed on the ABI 7900HT quantitative PCR system using the primer pairs as follows: ABCC2, forward, 5′-CAA GCA GGT GTT CGT CGT GT-3′, reverse, 5′-TAC GCC GCA TAA GAC CGA GA-3′, 232 bp; ACTB, forward, 5′-AAG ATC AAG ATC ATT GCT CCT CCT-3′, reverse, 5′-AGC TCA GTA ACA GTC CGC CT-3′, 171 bp. Relative quantification of ABCC2 mRNA expression was evaluated using the comparative cycle threshold (CT) method. The raw quantifications were respectively normalized to the ACTB value for each sample, and the relative expression levels of ABCC2 mRNA are shown as mean ± SD for three independent experiments with each in triplicate.

Statistical Analysis

All experiments in the current study were performed in triplicate. Statistical analyses were performed using GraphPad Prism (version 6.0). Data are expressed as the mean ± SD, and were analyzed by one-way ANOVA followed by a least significant difference (LSD) test. p values <0.05 were considered to be significant.

SUPPLEMENTAL INFORMATION

Supplemental Information can be found online at https://doi.org/10.1016/j.omtn.2019.12.023.

AUTHOR CONTRIBUTIONS

Y.Z. and N.L. engaged in study design and coordination, material support for obtained funding, and supervised the study. YZ. performed network analysis, designed the experimental validation, and wrote and revised the manuscript. X.M., W.C., and F.J. performed most of the experiments and statistical analyses and wrote the manuscript. The other authors performed parts of the experiments. All authors reviewed and approved the final manuscript.

CONFLICTS OF INTEREST

The authors declare that there is no conflict of interests regarding the publication of this paper.

ACKNOWLEDGMENTS

REFERENCES

1. Lotfi Shahreza, M., Ghadiri, N., Mousavi, S.R., Varshosaz, J., and Green, J.R. (2018). A review of network-based approaches to drug repositioning. Brief. Bioinform. *19*, 878–892.

2. Oprea, T.I., and Mestres, J. (2012). Drug repurposing: far beyond new targets for old drugs. AAPS J. *14*, 759–763.

3. Napolitano, F., Zhao, Y., Moreira, V.M., Tagliaferri, R., Kere, J., D'Amato, M., and Greco, D. (2013). Drug repositioning: a machine-learning approach through data integration. J. Cheminform. *5*, 30.

4. Li, J., Zheng, S., Chen, B., Butte, A.J., Swamidass, S.J., and Lu, Z. (2016). A survey of current trends in computational drug repositioning. Brief. Bioinform. *17*, 2–12.

5. Tan, F., Yang, R., Xu, X., Chen, X., Wang, Y., Ma, H., Liu, X., Wu, X., Chen, Y., Liu, L., and Jia, X. (2014). Drug repositioning by applying 'expression profiles' generated by integrating chemical structure similarity and gene semantic similarity. Mol. Biosyst. *10*, 1126–1138.

6. Silberberg, Y., Gottlieb, A., Kupiec, M., Ruppin, E., and Sharan, R. (2012). Large-scale elucidation of drug response pathways in humans. J. Comput. Biol. *19*, 163–174.

7. Jadamba, E., and Shin, M. (2016). A systematic framework for drug repositioning from integrated omics and drug phenotype profiles using pathway-drug network. BioMed Res. Int. *2016*, 7147039.

8. El-Serag, H.B. (2011). Hepatocellular carcinoma. N. Engl. J. Med. *365*, 1118–1127.

9. Torre, L.A., Bray, F., Siegel, R.L., Ferlay, J., Lortet-Tieulent, J., and Jemal, A. (2015). Global cancer statistics, 2012. CA Cancer J. Clin. *65*, 87–108.

10. Zhang, D.Y., and Friedman, S.L. (2012). Fibrosis-dependent mechanisms of hepato-carcinogenesis. Hepatology *56*, 769–775.

11. Xiang, Y., Guo, Z., Zhu, P., Chen, J., and Huang, Y. (2019). Traditional Chinese medicine as a cancer treatment: modern perspectives of ancient but advanced science. Cancer Med. *8*, 1958–1975.

12. Wang, J., Wong, Y.K., and Liao, F. (2018). What has traditional Chinese medicine delivered for modern medicine? Expert Rev. Mol. Med. *20*, e4.

13. Lin, A.X., Chan, G., Hu, Y., Ouyang, D., Ung, C.O.L., Shi, L., and Hu, H. (2018). Internationalization of traditional Chinese medicine: current international market, internationalization challenges and prospective suggestions. Chin. Med. *13*, 9.

14. Zhang, L.J., and Schuppan, D. (2014). Targeted therapy of liver fibrosis/cirrhosis and its complications. J. Hepatol. *61*, 166–168.

15. Dong, Q., Qiu, L.L., Zhang, C.E., Chen, L.H., Feng, W.W., Ma, L.N., Yan, D., Niu, M., Wang, J.B., and Xiao, X.H. (2016). Identification of compounds in an anti-fibrosis Chinese medicine (Fufang Biejia Ruangan pill) and its absorbed components in rat biofluids and liver by UPLC-MS. J. Chromatogr. B Analyt. Technol. Biomed. Life Sci. *1026*, 145–151.

16. Yang, F.R., Fang, B.W., and Lou, J.S. (2013). Effects of Fufang Biejia Ruangan pills on hepatic fibrosis in vivo and in vitro. World J. Gastroenterol. *19*, 5326–5333.

17. Yang, Y., Zhao, Y., Zhuang, H., Zhen, Z., Jiang, T., Li, L.K., and Chen, Y. (2018). Effect and mechanism of Fufang Biejia Ruangan tablet in prevention and treatment of rat hepatic fibrosis [in Chinese]. J. Guiyang Medical College *43*, 1380–1385.

18. Chai, M., Li, T.J., Cao, Y.J., Gen, Y.S., and Han, D. (2016). Effects on serum levels of IL-6, IL-8 and TNF-α and protective effects of liver injury by entecavir and Biejia Ruangan tablets in hepatitis B patients. Liaoning Zhongyiyao Daxue Xuebao *18*, 114–116.

19. Xu, H.Y., Zhang, Y.Q., Liu, Z.M., Chen, T., Lv, C.Y., Tang, S.H., Zhang, X.B., Zhang, W., Li, Z.Y., Zhou, R.R., et al. (2019). ETCM: an encyclopaedia of traditional Chinese medicine. Nucleic Acids Res. *47* (D1), D976–D982.

20. Keating, G.M. (2017). Sorafenib: a review in hepatocellular carcinoma. Target. Oncol. *12*, 243–253.

21. Personeni, N., Pressiani, T., Santoro, A., and Rimassa, L. (2018). Regorafenib in hepatocellular carcinoma: latest evidence and clinical implications. Drugs Context *7*, 212533.

22. Cheng, J.C., Chou, C.H., Kuo, M.L., and Hsieh, C.Y. (2006). Radiation-enhanced hepatocellular carcinoma cell invasion with MMP-9 expression through PI3K/Akt/NF-κB signal transduction pathway. Oncogene *25*, 7009–7018.

23. Li, Q., Wang, C., Wang, Y., Sun, L., Liu, Z., Wang, L., Song, T., Yao, Y., Liu, Q., and Tu, K. (2018). HSCs-derived COMP drives hepatocellular carcinoma progression by activating MEK/ERK and PI3K/AKT signaling pathways. J. Exp. Clin. Cancer Res. *37*, 231.

24. Hoffmann, A., Natoli, G., and Ghosh, G. (2006). Transcriptional regulation via the NF-κB signaling module. Oncogene *25*, 6706–6716.

25. Wang, S.S., Chen, Y.H., Chen, N., Wang, L.J., Chen, D.X., Weng, H.L., Dooley, S., and Ding, H.G. (2017). Hydrogen sulfide promotes autophagy of hepatocellular carcinoma cells through the PI3K/Akt/mTOR signaling pathway. Cell Death Dis. *8*, e2688.

26. Mazzoccoli, G., Miele, L., Oben, J., Grieco, A., and Vinciguerra, M. (2016). Biology, epidemiology, clinical aspects of hepatocellular carcinoma and the role of sorafenib. Curr. Drug Targets *17*, 783–799.

27. Villanueva, A., and Llovet, J.M. (2011). Targeted therapies for hepatocellular carcinoma. Gastroenterology *140*, 1410–1426.

28. Di Virgilio, F. (2014). Purinergic receptors in cancer and inflammation: from Rudolph Virchow to Geoff Burnstock. Purinergic Signal *10*, 657–658.

29. Ding, Y.F., Wu, Z.H., Wei, Y.J., Shu, L., and Peng, Y.R. (2017). Hepatic inflammation-fibrosis-cancer axis in the rat hepatocellular carcinoma induced by diethylnitrosamine. J. Cancer Res. Clin. Oncol. *143*, 821–834.

30. He, S., Yang, S., Niu, M., Zhong, Y., Dan Gao, Zhang, Y., Ma, H., Xiong, W., Zhou, M., Zhou, Y., et al. (2018). HMG-box transcription factor 1: a positive regulator of the G1/S transition through the Cyclin-CDK-CDKI molecular network in nasopharyngeal carcinoma. Cell Death Dis. *9*, 100.

31. Yang, C., Yao, C., Tian, R., Zhu, Z., Zhao, L., Li, P., Chen, H., Huang, Y., Zhi, E., Gong, Y., et al. (2019). miR-202-3p regulates Sertoli cell proliferation, synthesis function, and apoptosis by targeting LRP6 and cyclin D1 of Wnt/β-catenin signaling. Mol. Ther. Nucleic Acids *14*, 1–19.

32. Wishart, D.S., Feunang, Y.D., Guo, A.C., Lo, E.J., Marcu, A., Grant, J.R., Sajed, T., Johnson, D., Li, C., Sayeeda, Z., et al. (2018). DrugBank 5.0: a major update to the DrugBank database for 2018. Nucleic Acids Res. *46* (D1), D1074–D1082.

33. Zhang, Y.Q., Shen, Y., Liao, M.M., Mao, X., Mi, G.J., You, C., Guo, Q.Y., Li, W.J., Wang, X.Y., Lin, N., and Webster, T.J. (2019). Galactosylated chitosan triptolide nanoparticles for overcoming hepatocellular carcinoma: enhanced therapeutic efficacy, low toxicity, and validated network regulatory mechanisms. Nanomedicine (Lond.) *15*, 86–97.

34. Huang, L.K., and Wang, M.J.J. (1995). Image thresholding by minimizing the measures of fuzziness. Pattern Recognit. *28*, 41–51.

35. Handala, L., Fiore, T., Rouillé, Y., and Helle, F. (2019). QuantIF: an ImageJ macro to automatically determine the percentage of infected cells after immunofluorescence. Viruses *11*, 165.

36. Zhang, Y., Jiang, F., He, H., Ye, J., Mao, X., Guo, Q., Wu, S.L., Zhong, W., Wu, C.L., and Lin, N. (2018). Identification of a novel microRNA-mRNA regulatory biomodule in human prostate cancer. Cell Death Dis. *9*, 301.